

See discussions, stats, and author profiles for this publication at: <https://www.researchgate.net/publication/261915719>

Direct Detection and Speciation of Trace Explosives Using a Nanoporous Multifunctional Microcantilever

ARTICLE in ANALYTICAL CHEMISTRY · APRIL 2014

Impact Factor: 5.64 · DOI: 10.1021/ac500745g · Source: PubMed

CITATIONS

9

READS

66

4 AUTHORS, INCLUDING:



Dongkyu Lee

Korea Institute of Machinery and Materials

35 PUBLICATIONS 321 CITATIONS

[SEE PROFILE](#)



Seonghwan Kim

The University of Calgary

36 PUBLICATIONS 265 CITATIONS

[SEE PROFILE](#)



Thomas Thundat

University of Alberta

476 PUBLICATIONS 11,585 CITATIONS

[SEE PROFILE](#)

Direct Detection and Speciation of Trace Explosives Using a Nanoporous Multifunctional Microcantilever

Dongkyu Lee,^{*,†} Seonghwan Kim,^{†,‡} Sangmin Jeon,[§] and Thomas Thundat[†]

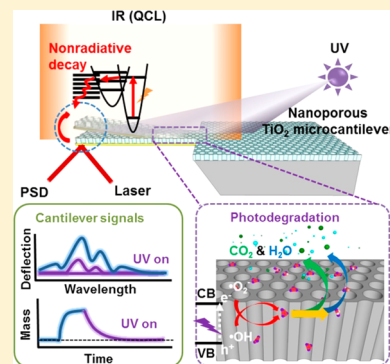
[†]Department of Chemical and Materials Engineering, University of Alberta, Edmonton, Alberta T6G 2 V4, Canada

[‡]Department of Mechanical and Manufacturing Engineering, University of Calgary, Calgary, Alberta T2N 1N4, Canada

[§]Department of Chemical Engineering, Pohang University of Science and Technology, Pohang, South Korea

Supporting Information

ABSTRACT: We have developed a highly selective and sensitive nanomechanical infrared (IR) calorimetric spectrometer for use in the direct detection of ultralow concentrations of explosive vapors using a nanoporous TiO₂ cantilever. These cantilevers were fabricated using a two-step anodization and photolithography process. By patterning nanoscale wells onto a cantilever, its surface area is increased by 2 orders of magnitude and the surface is converted into a preconcentrator. Resonant excitation of adsorbed molecules using IR radiation causes the cantilever to bend due to temperature changes originating from the nonradiative decay process. The porous structure of the cantilever increases its thermomechanical sensitivity as well as the number of adsorbed molecules. The system performance was demonstrated by detecting binary explosive mixtures under ambient conditions. The TiO₂ sensor surface also allows regeneration through the photocatalytic decomposition of adsorbates under UV irradiation.



Direct detection of trace explosives under ambient conditions is crucial to defeat terrorism but also presents a challenge due to extremely low vapor pressures of the explosives.^{1–6} For example, the vapor pressure of cyclotrimethylene trinitramine (RDX) is approximately 5 parts-per-trillion (ppt) at room temperature.³ Assuming that 10% of the impinging explosive molecules adsorb onto a sensor surface, the number of molecules adsorbed per second on a unit surface will be $3.5 \times 10^7/\text{cm}^2$. This estimate, which is 7 orders of magnitude less than the number of adsorption sites per cm^2 , is far below the detection limits of currently available miniaturized adsorption-based sensor platforms. Although techniques based on gas chromatography, mass spectroscopy, and vibrational spectroscopy have previously been shown to be capable of detecting explosive vapors at extremely low concentrations,^{7–9} they require time-consuming preprocessing steps and are not amenable to miniaturization in microsystems without performance degradation.

Microfabricated sensor platforms with chemoselective interfaces offer an ideal solution to the demand for miniaturized sensing systems.^{10–12} However, the selectivity of such systems is limited by the nonspecific nature of the chemical binding between a target and its receptor molecules. Recently, receptor-free nanomechanical infrared (IR) spectroscopy techniques have been developed to detect various molecules adsorbed onto a bimetallic cantilever.^{6,13–15} In this approach, IR absorption induced the deflection of the cantilever, providing a nanomechanical IR spectrum of the adsorbates. Despite the high selectivity attained using IR measurements, the sensitivity of the nanomechanical IR spectroscopy technique was not sufficient

for detection of very low concentrations of explosive vapors under ambient conditions.^{15–17}

To address this, we fabricated a novel cantilever directly from nanostructured TiO₂ substrates using a two-step anodization and photolithography process. Unlike conventional plain cantilevers, the nanoporous cantilever can act as a preconcentrator due to its large surface area. Compared to the nanoporous TiO₂-coated silicon microcantilever,^{18,19} the developed TiO₂ microcantilever was more flexible and produced a larger deflection upon IR absorption. Moreover, the sensor surface consisting of TiO₂ crystallites could be easily regenerated through photocatalytic decomposition of adsorbates under UV irradiation.

EXPERIMENTAL SECTION

Materials. Two standard explosive samples (trinitrotoluene (TNT) and RDX) were purchased from AccuStandard, Inc. (New Haven, CT) and were used without further purification. As indicated by the manufacturer, the standard concentration was 1 mg/mL. Phosphoric acid, nitric acid, chromic acid, perchloric acid, acetic acid, oxalic acid, and ethanol were purchased from Sigma-Aldrich (St. Louis, MO) and were used as received. A high-purity titanium sheet (99.7%) was obtained from Sigma-Aldrich. The photoresist (PR) AZ1512 and AZ developer CD30 were purchased from Clariant (Somerville, NJ) and were used for photolithography.

Received: February 25, 2014

Accepted: April 28, 2014

Published: April 28, 2014

Fabrication of the Nanoporous TiO₂ Microcantilevers. The schematic illustration of the fabrication process is described in Figure 1. A Ti foil was cleaned using ethanol

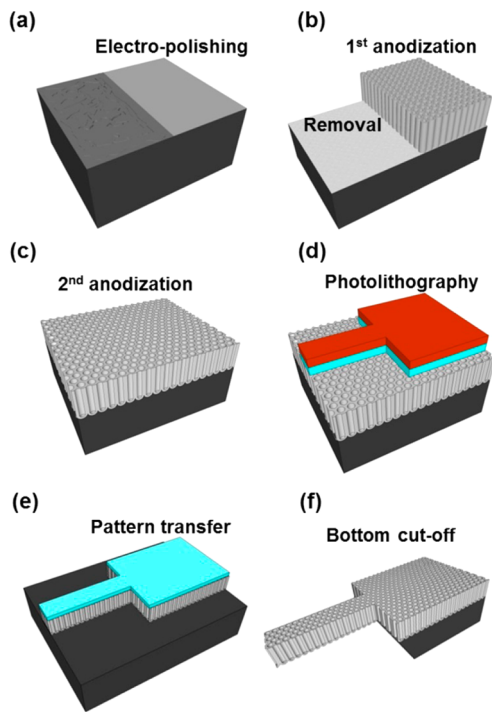


Figure 1. Schematic illustration of the fabrication process of a nanoporous TiO₂ microcantilever.

and acetone and was then electropolished in a mixture of perchloric acid (60%), butanol, and methanol (1:6:9 by vol %) at -20 °C by applying 20 V for 20 min (Figure 1a). The electropolished Ti foil was anodized in an ethylene glycol solution containing NH₄F (0.38 wt %) and H₂O (1.79 wt %) and placed in a well-insulated bath for 3 h at 30 V at 15 °C using a dc power supply.^{20,21} The first anodization resulted in the formation of nanotubes on the substrate and then followed by ultrasonication in water for 30 min to remove the nanotubes (Figure 1b). A second anodization was then conducted for 1 h under the same conditions as the first anodization, producing hexagonally well-ordered nanopores on the Ti foil (Figure 1c). After the second anodization step, the sample was washed with distilled water and ethanol and dried off using N₂ gas. To pattern cantilevers on the nanoporous TiO₂ layer, a 500 nm thick transfer layer of aluminum was deposited using thermal evaporation. The photoresist (PR) was patterned by simple photolithography (Figure 1d). The unprotected aluminum was removed using an aluminum etching solution (H₃PO₄/CH₃COOH/HNO₃/H₂O = 16:1:1:2 by wt %) for 20 min. The nanoporous TiO₂ layers not covered by the PR were wet-etched in 5 wt % of hydrofluoric acid in 1 M sodium phosphate at room temperature for 30 s. The remaining PR on the aluminum layer was removed by rinsing with acetone (Figure 1e). The formed nanopores have an amorphous structure but can be converted into anatase through annealing at 500 °C for 2 h with a heating and cooling rate of 1.7 °C/min in N₂. The bottom cutoff was then carried out under the electropolishing conditions for 60 min in order to produce free-standing cantilever structures. The remaining aluminum on the nano-

porous TiO₂ layer was removed using the aluminum etching solution (Figure 1f).

In Situ Gas Flow Setup. Vapor samples were introduced by passing dry air at a fixed flow rate of 50 mL/min (the carrier gas) through simple vapor generators (tubes with quartz wool heated to specific temperatures appropriate for each of TNT and RDX). The vapors were generated at room temperature (22 °C in the laboratory) as well as at a specific temperature appropriate for RDX or TNT. The final vapor concentration at the elevated temperature was calculated to be from ~2.5 ppt (22 °C) to 130 ppb (100 °C) for RDX and from ~4.5 ppb (22 °C) to 65 ppb (40 °C) for TNT.²²

Nanomechanical IR Spectroscopy Setup. The experimental setup used in this study is shown in Figure 2. Typical

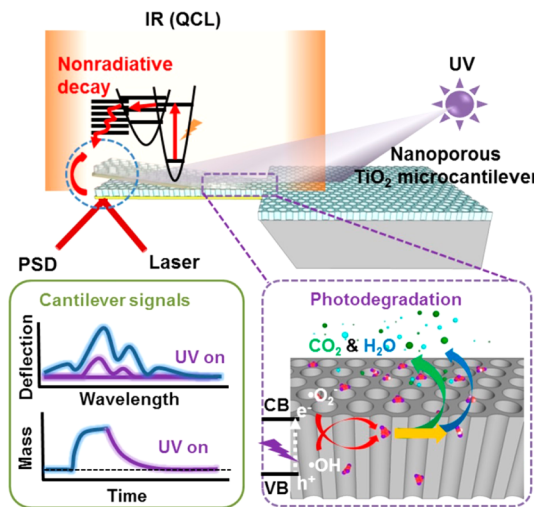


Figure 2. Schematic illustration of a multifunctional, gold-coated nanoporous TiO₂ cantilever for use in nanomechanical IR spectroscopy and photodegradation of adsorbed molecules.

dimensions of the nanoporous TiO₂ cantilevers used in our experiments were 350 μm in length, 50 μm in width, and 3 μm in thickness. The nanowell-patterned TiO₂ microcantilever was coated with 5 nm titanium and 50 nm gold using a thermal evaporator to enhance thermomechanical sensitivity. The gold-coated nanoporous TiO₂ cantilever was used for the experiments and was initially mounted inside a quartz flow cell. The nanomechanical IR spectra were collected by attaching the quartz flow cell to the head unit of a MultiMode atomic force microscope (Bruker, Santa Barbara, CA). The deflection and resonance frequencies of the microcantilever were monitored using the optical beam deflection method with a laser diode and a position-sensitive detector. The intensity of the 200 kHz pulsed IR radiation with a 10% duty cycle from the quantum cascade laser (Daylight Solutions ÜT-8) was electrically modulated at 20 Hz using a function generator DS345 (Stanford Research Systems, Sunnyvale, CA) and was directed to the cantilever. The IR wavelength was scanned from 7.1 to 8.73 μm (1408 cm⁻¹ to 1145 cm⁻¹) using a ÜT-8 with a step size of 5 nm. The nanomechanical IR spectra were recorded using an SR850 lock-in amplifier (Stanford Research Systems, Sunnyvale, CA), and the resonance frequencies of the microcantilever were measured using an SR760 spectrum analyzer (Stanford Research Systems, Sunnyvale, CA). The mechanism by which the thermally sensitive microcantilever deflected under pulsed IR light is described in detail in our

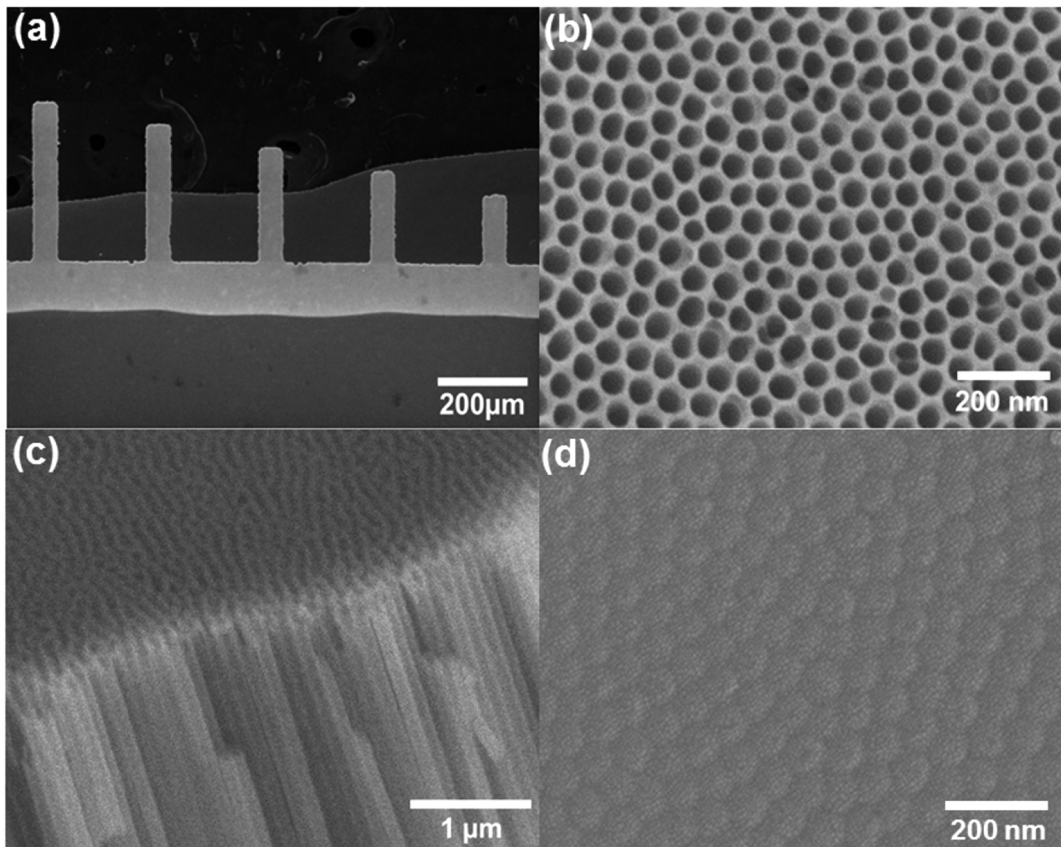


Figure 3. (a) SEM image of nanoporous TiO_2 microcantilevers with different lengths ranging from 150 to 350 μm , in 50 μm increments. Top-view (b), side-view (c), and back side-view (d) SEM images of the nanowells.

previous publication.⁶ In brief, the resonant excitation of specific molecular bonds at a specific wavelength introduces nonradiative decay process-induced phonons which increase the temperature of the cantilever, resulting in its deflection. The unique photocatalytic properties of the TiO_2 impart a self-cleaning functionality to the cantilever which regenerates the surface. Irradiation of the surface-adsorbed molecules with UV light ($\lambda = 254 \text{ nm}$, 4.5 mW/cm^2 , Spectroline, NY) varies both the nanomechanical IR spectrum and the adsorbed mass due to the photocatalytic degradation of the adsorbed molecules. The mechanism by which the TiO_2 sensors undergo self-cleaning has been reported elsewhere.^{23,24}

RESULTS AND DISCUSSION

Figure 3a–d shows scanning electron microscopy images of nanoporous TiO_2 microcantilevers at different magnifications. Five cantilevers with various lengths (150–350 μm) are shown in Figure 3a. These cantilevers contained ordered nanopores with an average diameter of 55 nm and a pore-to-pore distance of 77 nm, as shown in Figure 3b,c. The bottom side of each cantilever was sealed by a titanium oxide barrier layer so that each pore was U-shaped as shown in Figure 3d. The depth of the nanowells was ~3 μm . The surface area of a nanoporous TiO_2 cantilever was approximately 2 orders of magnitude larger than that of a plain microcantilever with identical dimensions. The effective Young's modulus of the TiO_2 cantilever was determined to be ~6 GPa, 28 times smaller than that of a silicon cantilever due to the high porosity.²⁵ The spring constant of a TiO_2 cantilever having dimensions of 350 μm in length, 50 μm in width, and 3 μm in thickness was determined

to be ~0.051 N/m. Thermomechanical sensitivity was enhanced by applying a gold coating to the bottom layer of the cantilever (a gold-coated nanoporous TiO_2 cantilever). The thickness of the gold layer that optimized bending upon IR absorption was calculated to be ~50 nm.²⁶ A control experiment was conducted using a bimetallic silicon microcantilever characterized by a comparable spring constant and planar dimensions. The thermomechanical sensitivity of the 50 nm gold-coated nanoporous TiO_2 cantilever (~610 nm/K) was much higher than that of the 200 nm gold-coated silicon cantilever (~195 nm/K), as shown in Figure 4a. The IR response of the gold-coated nanoporous TiO_2 cantilever was 7 times higher than that of the gold-coated Si microcantilever, as shown in Figure 4b.

Figure 5a,b shows the characteristic nanomechanical IR absorption peaks of RDX and TNT molecules adsorbed onto a gold-coated nanoporous TiO_2 cantilever at various vapor concentrations. The nanomechanical IR peaks corresponding to RDX and TNT were clearly observed even at room temperature. The nanomechanical IR spectra of RDX and TNT shown in Figure 5a,b are consistent with the corresponding conventional IR absorption spectra. The RDX peaks at 7.58 μm , 7.86 μm , and 8.16 μm were attributed to the symmetric stretching of the NO_2 (nitro) group bonds with the nitrogen atom ($\text{N}-\text{NO}_2$), and the TNT peak at 7.42 μm was attributed to the symmetric stretching of the NO_2 (nitro) group bonds with carbon ($\text{C}-\text{NO}_2$).^{27,28} The RDX and TNT peak intensities gradually increased as a function of the vapor concentration. The limit of detection (LOD) of the RDX and TNT vapor concentrations with a collection time of 3 min was

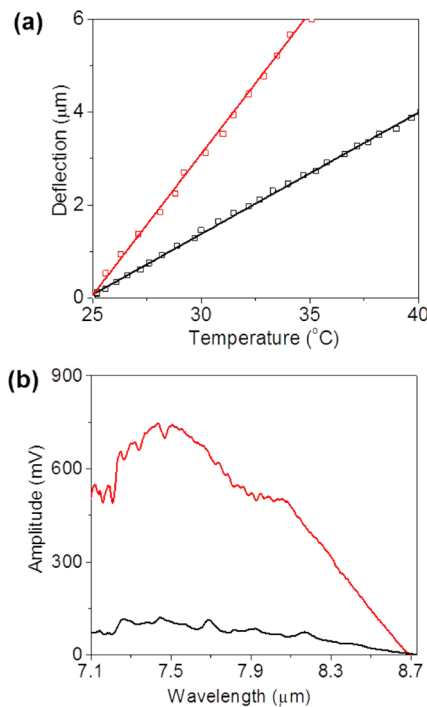


Figure 4. Thermomechanical sensitivities (a) and IR responses (b) of the 50 nm gold-coated nanoporous TiO_2 microcantilever (red line) and the 200 nm gold-coated Si microcantilever which has a comparable spring constant and planar dimensions (black line).

estimated to be approximately 300 parts-per-quadrillion (ppq) at 7.58 μm and 800 ppt at 7.42 μm , respectively, as shown in Figure 5c. The LOD for TNT and RDX was determined by the intersection of the straight line and the dashed line with a

standard deviation of 3 at the wavelength. The different LOD values were attributed to differences in the IR peak intensities at the characteristic wavelengths and differences in the amounts of adsorbed molecules present on the cantilever. The sticky RDX molecules accumulated on the cantilever surface over time,²⁹ whereas fewer TNT molecules adsorbed onto the cantilever surface due to the high rate of TNT desorption during sample injection (see Figure S1 in the Supporting Information). Figure 5d shows the nanomechanical IR spectrum of a binary mixture of explosive vapors (RDX and TNT) with a 1 to 1 mass ratio, acquired at room temperature (22 $^{\circ}\text{C}$) with a collection time of 3 min. The mixture spectrum is the linear superposition of the individual spectrum; therefore, several distinguishable peaks appear in the binary mixture spectrum.⁶

Figure 6a shows the real-time mass loading of RDX molecules onto the nanoporous TiO_2 microcantilever at a vapor concentration of 130 ppb for 4 min. The adsorption of 130 ppb RDX molecules onto the nanoporous TiO_2 surface (red) was characterized by two different rate constants: 11.3 pg/s during the early stages and 6.5 pg/s during the later stages. However, the rate of RDX adsorption at a constant vapor concentration onto a plain Si surface (black) was approximately 1.1 pg/s, indicating that RDX molecules could be rapidly adsorbed onto the nanoporous TiO_2 surface due to its large surface area. The observed increase, a factor of 10, in the rate of adsorption does not scale with the 2 orders of magnitude increase in surface area probably due to slow diffusion of RDX vapors into the nanowell. The peak amplitude of the gold-coated nanoporous TiO_2 cantilever was 176 times higher than that of the gold-coated Si microcantilever at the same vapor concentration and collection time, as shown in Figure 6b. Moreover, the gold-coated plain Si microcantilever could not detect RDX molecules at ultralow vapor concentrations.

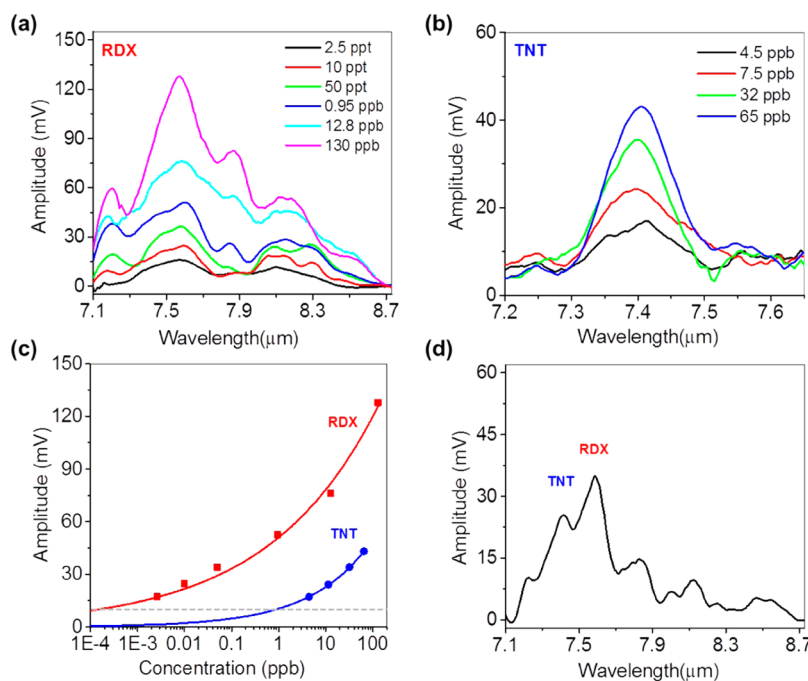


Figure 5. (a) Nanomechanical IR spectra of RDX molecules, collected for 3 min at various vapor concentrations: 2.5 ppt (22 $^{\circ}\text{C}$, black), 10 ppt (30 $^{\circ}\text{C}$, red), 50 ppt (40 $^{\circ}\text{C}$, green), 0.95 ppb (60 $^{\circ}\text{C}$, blue), 12.8 ppb (80 $^{\circ}\text{C}$, cyan), and 130 ppb (100 $^{\circ}\text{C}$, magenta). (b) Nanomechanical IR spectra of TNT molecules collected for 3 min at various vapor concentrations: 4.5 ppb (22 $^{\circ}\text{C}$, black), 7.5 ppb (28 $^{\circ}\text{C}$, red), 32 ppb (35 $^{\circ}\text{C}$, green), and 65 ppb (40 $^{\circ}\text{C}$, blue). (c) Peak amplitudes at 7.58 μm for RDX (red) and 7.42 μm for TNT (blue) as a function of each vapor concentration. (d) Nanomechanical IR spectra of the binary mixture of RDX and TNT molecules collected for 3 min at room temperature (22 $^{\circ}\text{C}$).

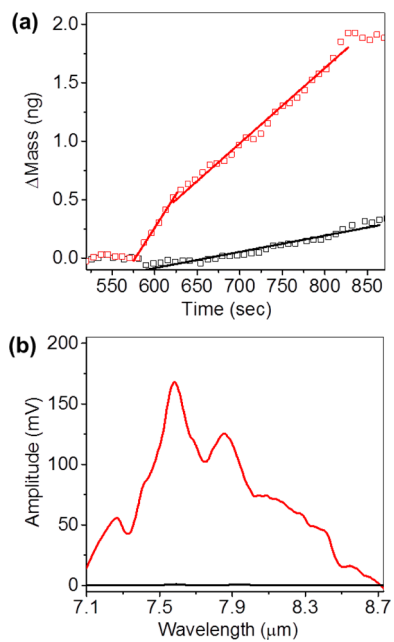


Figure 6. (a) Mass of RDX molecules adsorbed at 130 ppb onto the nanoporous TiO_2 cantilever (red squares) or the plain Si cantilever (black squares). Red and black straight lines indicate the linear fits of the adsorbed mass, giving the adsorption rate constants. (b) Nanomechanical IR spectra of the RDX molecules adsorbed onto a gold-coated TiO_2 (red) or a gold-coated Si microcantilever (black).

The sensor surface was regenerated by photocatalytically cleaving the RDX molecules.^{30,31} Figure 7a shows a rapid decrease in the adsorbed mass due to the photocatalytic decomposition upon irradiation of the anatase phase TiO_2 cantilever with UV light. The control experiment conducted with a gold-coated Si cantilever displayed a slight decrease in the mass as a result of the UV-induced direct photolysis of nitramines; however, the extent of photolysis was very small compared to the mass changes observed on the TiO_2 cantilever. The noise in the mass measurements was higher in the nanomechanical IR spectra of RDX collected using pulsed, rather than constant, IR light. The series of spectra shown in Figure 7b indicates that the characteristic RDX peaks changed during the photolytic desorption and photocatalytic decomposition of RDX. The main RDX peak at $7.58\ \mu\text{m}$ is dramatically decreased when irradiated with UV light. Longer times were needed to completely eliminate the molecular vibrational peaks of the nitro group bonds due to the low power of the UV source used in our experiments ($\lambda = 254\ \text{nm}$, $4.5\ \text{mW}/\text{cm}^2$).

Figure 7c shows that the logarithmic decrease in the normalized mass and amplitude of the RDX peaks at $7.58\ \mu\text{m}$ during photodegradation was linear with respect to the UV-irradiation time, indicating that the RDX photodegradation followed pseudo-first-order kinetics.¹⁹ The apparent first-order rate constants calculated from the gradients of the mass changes, k_{m} , were ~ 0.027 and $0.009\ \text{min}^{-1}$ for the TiO_2 and Si cantilevers, respectively, confirming that photocatalytic decomposition was much faster than photolytic cleavage. The rate constant calculated from the gradients of the peak intensity changes at $7.58\ \mu\text{m}$, k_{p} , was $\sim 0.029\ \text{min}^{-1}$ for the TiO_2 cantilever, similar to the rate constant calculated from the mass gradient.

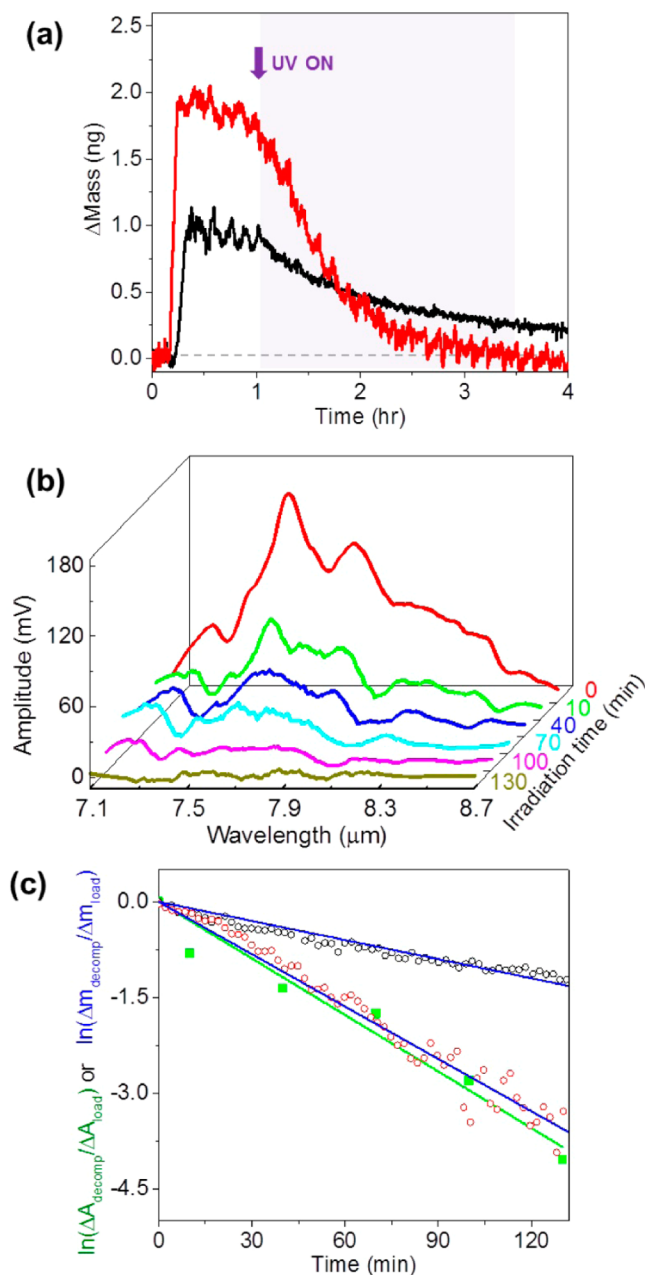


Figure 7. (a) Mass change of RDX molecules adsorbed on the gold-coated nanoporous TiO_2 (red) or gold-coated Si (black) microcantilevers during adsorption and photodegradation. (b) Nanomechanical IR spectra of RDX as a function of the UV irradiation time: 0 h (red), 10 min (green), 40 min (blue), 70 min (cyan), 100 min (magenta), and 130 min (dark yellow). (c) Logarithmic plot of the normalized mass during the photocatalytic or photolytic degradation of the RDX molecules adsorbed onto the nanoporous TiO_2 (red open circles) or plain Si (black open circles) cantilever. A logarithmic plot of the normalized nanomechanical IR peak intensities at $7.58\ \mu\text{m}$, obtained during the photocatalytic degradation of RDX molecules on the nanoporous TiO_2 surface (closed green squares).

CONCLUSIONS

In summary, we developed a novel sniffer with high sensitivity and selectivity based on nanomechanical IR spectroscopy using a nanowell-patterned TiO_2 microcantilever. The presence of nanowells increased the surface area of the cantilever by 2 orders of magnitude and enhanced the sensitivity of the system substantially when applied to the detection of a binary mixture

of explosive molecules. The system developed here satisfies three essential criteria required for high-performance chemical sensing: preconcentration of analytes, chemical selectivity, and sensitivity. The photocatalytic sensor surface could be easily regenerated after each adsorption measurement by irradiating it with UV light. The nanoporous TiO₂ cantilevers also show great potential for use in a variety of applications such as an electronic nose, uncooled miniature IR detectors for IR imaging, and nanoscale in situ chemical and biological reactors.

■ ASSOCIATED CONTENT

Supporting Information

Graph showing the variations in the adsorbed mass of TNT and RDX on the nanoporous TiO₂ microcantilever (Figure S1). This material is available free of charge via the Internet at <http://pubs.acs.org>.

■ AUTHOR INFORMATION

Corresponding Author

*E-mail: dongkyu@ualberta.ca.

Notes

The authors declare no competing financial interest.

■ ACKNOWLEDGMENTS

This work was supported by the Canada Excellence Research Chairs (CERC) Program. D.L. also would like to acknowledge the support from Basic Science Research Program through the National Research Foundation of Korea (NRF) funded by the Ministry of Education, Science and Technology (Grant 2012R1A6A3A03040416).

■ REFERENCES

- (1) Yinon, J. *Anal. Chem.* **2003**, *75*, 99A–105A.
- (2) Naddo, T.; Che, Y.; Zhang, W.; Balakrishnan, K.; Yang, X.; Yen, M.; Zhao, J.; Moore, J. S.; Zang, L. *J. Am. Chem. Soc.* **2007**, *129*, 6978–6979.
- (3) Ewing, R. G.; Atkinson, D. A.; Clowers, B. H. *Anal. Chem.* **2013**, *85*, 389–397.
- (4) Bonnot, K.; Bernhardt, P.; Hassler, D.; Baras, C.; Comet, M.; Keller, V.; Spitzer, D. *Anal. Chem.* **2010**, *82*, 3389–3393.
- (5) Wang, J.; Yang, L.; Boriskina, S.; Yan, B.; Reinhard, B. M. *Anal. Chem.* **2011**, *83*, 2243–2249.
- (6) Kim, S.; Lee, D.; Liu, X.; Neste, C. V.; Jeon, S.; Thundat, T. *Sci. Rep.* **2013**, *3*, 1111.
- (7) Fainberg, A. *Science* **1992**, *255*, 1531–1537.
- (8) Kolla, P. *Angew. Chem., Int. Ed.* **1997**, *36*, 800–811.
- (9) Moore, D. S. *Rev. Sci. Instrum.* **2004**, *75*, 2499–2512.
- (10) Hsieh, M.-D.; Zellers, E. T. *Anal. Chem.* **2004**, *76*, 1885–1895.
- (11) Jin, C.; Kurzawski, P.; Hierlemann, A.; Zellers, E. T. *Anal. Chem.* **2008**, *80*, 227–236.
- (12) Zhao, W.; Pinnaduwage, L. A.; Leis, J. W.; Gehl, A. C.; Allman, S. L.; Shepp, A.; Mahmud, K. K. *J. Appl. Phys.* **2008**, *103*, 104902–1–104902–11.
- (13) Barnes, J. R.; Stephenson, R. J.; Welland, M. E.; Gerber, Ch.; Gimzewski, J. K. *Nature* **1994**, *372*, 79–81.
- (14) Li, G.; Burggraf, L. W.; Baker, W. P. *Appl. Phys. Lett.* **2000**, *76*, 1122–1124.
- (15) Krause, A. R.; Van Neste, C.; Senesac, L.; Thundat, T.; Finot, E. *J. Appl. Phys.* **2008**, *103*, 094906–1–094906–6.
- (16) Datskos, P. G.; Sepaniak, M. J.; Tipple, C. A.; Lavrik, N. *Sens. Actuators, B* **2001**, *76*, 393–402.
- (17) Datskos, P. G.; Rajic, S.; Sepaniak, M. J.; Lavrik, N.; Tipple, C. A.; Senesac, L. R.; Datskou, I. *J. Vac. Sci. Technol. B* **2001**, *19*, 1173–1179.
- (18) Spitzer, D.; Cottineau, T.; Piazzon, N.; Josset, S.; Schnell, F.; Pronkin, S. N.; Savinova, E. R.; Keller, V. *Angew. Chem., Int. Ed.* **2012**, *51*, 5334–5338.
- (19) Joo, J.; Shim, J.; Seo, H.; Jung, N.; Wiesner, U.; Lee, J.; Jeon, S. *Anal. Chem.* **2010**, *82*, 3032–3037.
- (20) Shin, Y.; Lee, S. *Nano Lett.* **2008**, *8*, 103171–103173.
- (21) Wang, D.; Liu, Y.; Yu, B.; Zhou, F.; Liu, W. *Chem. Mater.* **2009**, *21*, 1198–1206.
- (22) Ostmark, H.; Wallin, S.; Ang, H. G. *Propellants, Explos., Pyrotech.* **2012**, *37*, 12–23.
- (23) Hoffmann, M. R.; Martin, S. T.; Choi, W. Y.; Bahnemann, D. W. *Chem. Rev.* **1995**, *95*, 69–96.
- (24) Linsebigler, A. L.; Lu, G. Q.; Yates, J. T. *Chem. Rev.* **1995**, *95*, 735–758.
- (25) Lee, D.; Shin, N.; Lee, K.-H.; Jeon, S. *Sens. Actuators, B* **2009**, *137*, 561–565.
- (26) Lai, J.; Perazzo, T.; Shi, Z.; Majumdar, A. *Sens. Actuators, A* **1997**, *58*, 113–119.
- (27) Priester, F.; Halik, M.; Castelli, A.; Fredericks, W. *Anal. Chem.* **1960**, *32*, 495–508.
- (28) Lewis, I. R.; Daniel, N. W., Jr.; Griffiths, P. R. *Appl. Spectrosc.* **1997**, *51*, 1854–1867.
- (29) Pinnaduwage, L. A.; Thundat, T.; Gehl, A.; Wilson, S. D.; Hedden, D. L.; Lareau, R. T. *Ultramicroscopy* **2004**, *100*, 211–216.
- (30) Andrew, T. L.; Swager, T. M. *J. Org. Chem.* **2011**, *76*, 2976–2993.
- (31) Choi, J.-K.; Son, H.-S.; Kim, T.-S.; Stenstrom, M. K.; Zoh, K.-D. *Environ. Technol.* **2006**, *27*, 219–232.